TALLINN UNIVERSITY OF TECHNOLOGY
SCHOOL OF ENGINEERING
Department of Materials and Environmental Technology

DOPING OF ANTIMONY SELENIDE THIN FILMS BY CATION EXCHANGE

ANTIMONSELENIIDI ÕHUKESTE KILEDE DOPEERIMINE KATIOONVAHETUSE MEETODIL

MASTER THESIS

Student: Ivan Kuznietsov

Student code: 213852KAYM

Supervisor: Dr. Svetlana Polivtseva

Co-supervisor: Dr. Olga Volobujeva

Tallinn 2023

AUTHOR'S DECLARATION

Hereby I declare, that I have written this thesis independently.
No academic degree has been applied for based on this material. All works, major viewpoints and data of the other authors used in this thesis have been referenced.

"....." ..... 20…..

Author: .....
/signature /

Thesis is in accordance with terms and requirements

"....." ..... 20….

Supervisor: ….....
/signature/

Accepted for defence

"....."..... 20… .

Chairman of theses defence commission: .....
/name and signature/

Non-exclusive Licence for Publication and Reproduction of GraduationTthesis[1]

I, _____ (name of the author) (date of birth: ……..) hereby

1. grant Tallinn University of Technology (TalTech) a non-exclusive license for my thesis

_____
_____
_____
_____,

(*title of the graduation thesis*)

supervised by

_____,

(*Supervisor's name*)

1.1 reproduced for the purposes of preservation and electronic publication, incl. to be entered in the digital collection of TalTech library until expiry of the term of copyright;

1.2 published via the web of TalTech, incl. to be entered in the digital collection of TalTech library until expiry of the term of copyright.

1.3 I am aware that the author also retains the rights specified in clause 1 of this license.

2. I confirm that granting the non-exclusive license does not infringe third persons' intellectual property rights, the rights arising from the Personal Data Protection Act or rights arising from other legislation.

---

[1] *Non-exclusive Licence for Publication and Reproduction of Graduation Thesis is not valid during the validity period of restriction on access, except the university`s right to reproduce the thesis only for preservation purposes.*

_____ (*signature*)

_____ (*date*)

Department of Materials and Environmental Technology

THESIS TASK

Student: Ivan Kuznietsov, 213852KAYM

Study programme, KAYM - Materials and Processes for Sustainable Energy

main speciality: Materials for Sustainable Energy

Supervisor(s): Researcher, Dr. Svetlana Polivtseva, 6203368, Senior Researcher, Dr. Olga Volobujeva, 6203368

Thesis topic:

(in English) Doping of antimony selenide thin films by cation exchange.

(in Estonian) Antimonseleniidi õhukeste kilede dopeerimine katioonvahetuse meetodil.

Thesis main objectives:

1. To investigate the applicability of cation exchange to dope Sb_2Se_3 thin films.

2. To develop an efficient cation exchange doping procedure using Ag as a dopant.

Thesis tasks and time schedule:

No	Task description	Deadline
1.	Literature research	
3.	Finding the conditions suitable for Ag doping of Sb_2Se_3 films and conducting experiments.	
4.	Characterization of the treated samples by SEM/EDX, XRD, Raman, UV-vis spectroscopy, PL	
5.	Reporting and composing the thesis	

Language: English **Deadline for submission of thesis:** "24" May 2023

Student: Ivan Kuznietsov ..... "....." May 2023
/signature/

Supervisor: Svetlana Polivtseva ..... "....." May 2023
/signature/

Co-supervisor: Olga Volobujeva ..... "....." May 2023
/signature/

Head of study programme: Sergei Bereznev ..... "....." May 2023
/signature/

CONTENTS

PREFACE

The thesis of this thesis was proposed by my supervisors Dr. Svetlana Polivtseva and Dr. Olga Volobujeva. This work was carried out in the Laboratory of Photovoltaic Materials of Tallinn University of Technology.

This work investigates the applicability of cation exchange for doping of antimony (III) selenide thin films. Reaction was carried out using a silver dopant source and complexing chemical – sodium bicarbonate ($NaHCO_3$) in glycerol at 210 ^oC. The results indicate a strong influence of complexing chemicals on dopant concentration in the final sample. A successful utilisation of $NaHCO_3$ in combination with Ag source for doping of the thin film was reported, same as undesirable phase formation in case of avoiding the usage of a complexing agent. Multiple characterisation techniques were used to study surface, cross sections, elemental composition, structural, optical properties and defects to draw conclusions.

I would like to express gratitude to my supervisor Svetlana Polivtseva for guiding me to the research topic, dedicating a lot of time and patience and sharing her knowledge, experience and unique vision with me. I also am very grateful to Olga Volobujeva for introducing characterisation techniques like SEM and UV-Vis to me, assisting in the literature research and providing SEM images for this work. By working on this thesis, I had a chance to see thin film and sustainable energy technologies from a unique angle and get in contact with novel approaches and ideas. Additionally, I would like to express special gratitude to Dr. Sergei Bereznev for being open and helpful on any matter throughout my whole journey of master's studies.

Keywords: Sb_2Se_3, thin films, doping, cation exchange, ion exchange

List of abbreviations and symbols

CIGS	Copper indium gallium selenide
CZTS	Copper zinc tin selenide
PV	Photovoltaic
CSS	Close-spaced sublimation
CBD	Chemical bath deposition
CSP	Chemical spray pyrolysis
ALD	Atomic layer deposition
RF	Radiofrequency
PEC	Photoelectrochemical water splitting
STH	Solar-to-hydrogen
AER	Anion exchange reaction
CER	Cation exchange reaction
SEM	Scanning electron microscopy
EDX	Energy-dispersive X-ray
XRD	X-ray Diffraction
PL	Photoluminescence
UV-Vis	Ultraviolet-visible spectroscopy
TEM	Transmission electron microscopy
STEM	Scanning transmission electron microscopy
FTO	Fluorine-doped tin oxide
ICDD	The International Centre for Diffraction Data
V_{OC}	Open-circuit voltage

INTRODUCTION

Our society is dependent on energy sources for continuing socioeconomic development, yet the sources of energy and the supply chains associated with them are not currently reliable and lead to energy crises. The current energy situation in the European Union is shaped by two significant aspects. Firstly, a set of policy initiatives - the European Green Deal with a final goal of climate neutrality by 2050, approved in 2020, demonstrates the commitment of the region to a sustainable future and a low-carbon economy transition [1]. Secondly, the energy landscape is currently facing additional challenges in the hydrocarbon supply chain crisis due to Russia's invasion of Ukraine. This crisis intensifies the pressure put on European energy initiatives and calls for diverse and clean energy sources to ensure the region's stability and security [2].

The growing global demand for clean energy sources, such as solar cells and hydrogen production, has spurred extensive research in the area [3]. Scientists have been investigating new functional materials and their application in various solar cell structures, as the efficiency of existing silicon-based solar cells, which are widely used yet relatively expensive and energy-intensive in manufacturing, is approaching its theoretical limits. The cost of production plays a significant role in determining the development of new, highly efficient, and cost-effective solar cell devices. Therefore, polycrystalline thin-film solar cells that utilize less absorber material have emerged as an appealing alternative. Materials like copper indium gallium selenide (CIGS), cadmium telluride (CdTe) and copper zinc tin sulfide (CZTS) along with suitable buffer layers, have shown high efficiencies of 23.35%, 22.1% and 12.6% and have successfully entered commercial market. [4][5][6]. As early as 2004 thin films obtained tangible solar cell market share, peaking at ~14% in 2009 and declining ever since with ~5% share in 2021 mainly by CdTe and CIGS [7][8]. Due to the toxicity of Cd and scarcity of Te, In and Ga alternative materials can be a solution for bottlenecks faced by the industry.

Antimony (III) selenide is a stable, relatively earth-abundant and less toxic absorber material currently studied as an alternative to CdTe and CIGS with a record efficiency of 10.57% to date, after slightly more than a decade since first attempts [9][10]. At the current stage of development, the electrical properties of Sb_2Se_3 are hard to control and thus films often form p-, n-type or intrinsic semiconductor material, due to hard defect chemistry and the presence of undesired phases associated with the established deposition methods [11][12]. Doping is often suggested as a prosperous technique to improve the optoelectronic properties of antimony selenide. This area is not that well

studied and only a few successful attempts at improving film properties were demonstrated with doping.

This work aims to test the applicability of cation exchange in the context of Sb_2Se_3 thin film doping. The atoms of silver are introduced to the lattice of antimony selenide via a simple, scalable and cheap solution-based method. This is the first reported attempt at doping Sb_2Se_3 thin films with silver via cation exchange.

1. LITERATURE REVIEW

1.1 Sb_2Se_3

Antimony selenide has brought increased research attention as an emerging less toxic, cheap and relatively earth-abundant semiconducting material with high potential for photovoltaic (PV) solar energy harvesting applications.

1.1.1 Phase diagram, structure and properties

Sb_2Se_3 is a binary compound of Sb and Se. Antimony (Sb) is a member of the 15th group with an electronegativity of 2.05, while selenium (Se) is from the 16th group with an electronegativity of 2.55. In Sb_2Se_3 oxidation states of atoms are +3 and -2 accordingly.

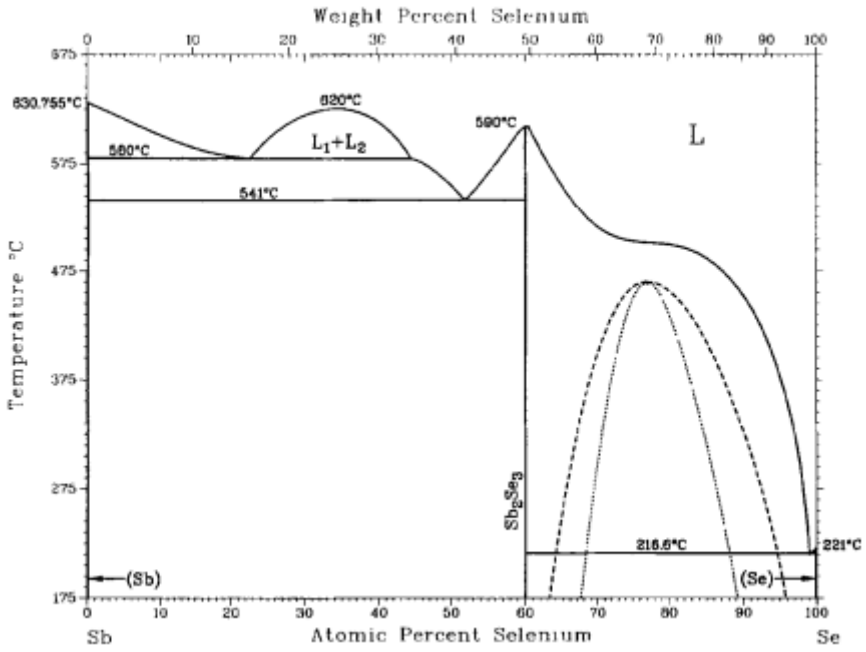

Figure 1.1 Sb-Se phase diagram [13]

A combination of 40% Sb and 60% Se yields the Sb_2Se_3 phase at a temperature range from 175°C to 590 °C. The formation of other phases is less probable in this concentration region [13].

Sb_2Se_3 has a one-dimensional (1D) crystal structure, consisting of $[Sb_4Se_6]_n$ ribbons held together by Se-Se weak Van der Waals interactions, while its unit cell has an orthorhombic structure and belongs to the Pnma space group, $[Sb_4Se_6]_n$ units are aligned along the c-axis in the direction of [001]. Figure 1.2 shows the representation of the crystal structure [14].

Antimony (III) selenide is a promising absorber material due to its bandgap varying between 1.0 - 1.3 eV and high absorption coefficient exceeding 10^5 cm^{-1} [15][14]. Antimony selenide has a very complex defect structure, thus the conductivity type can vary from n-type to p-type [11]. Experimental samples of pure antimony selenide more resemble a weak p-type conductivity. However, the presence of intrinsic and extrinsic defects such as introduced Cl, I or Cd atoms often make it an n-type semiconductor [16][17][18][19]. To stabilize the electrical properties of Sb_2Se_3, different approaches for doping have been suggested.

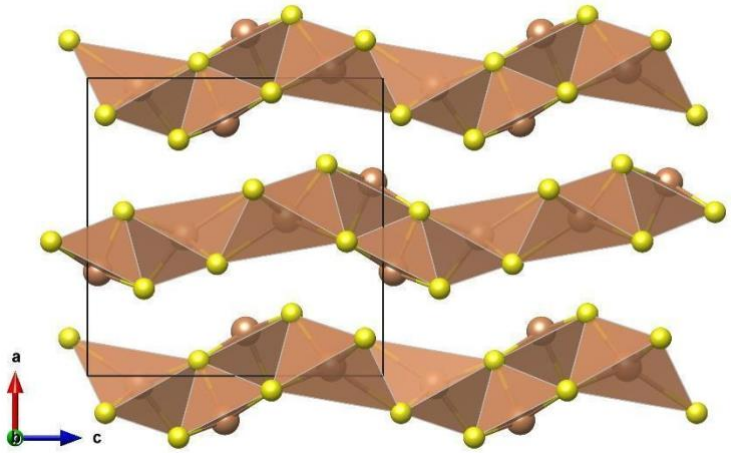

Figure 1.2 Sb_2Se_3 crystal structure. The orthorhombic unit cell is outlined by the black line. Sb and Se are represented by brown and yellow balls respectively [20]

1.2 Deposition methods

Antimony selenide films can be deposited by various processes. The most important physical deposition techniques in the industry are close-spaced sublimation (CSS), magnetron sputtering, and thermal evaporation, while chemical bath deposition (CBD), chemical spray pyrolysis (CSP) and atomic layer deposition (ALD) are common among chemical ones.

1.2.1 Physical deposition methods

Close-spaced sublimation (CSS) is one of the most common ways to deposit Sb_2Se_3 thin films, often yielding high efficiencies in optoelectronic devices. This fast and cost-effective technique is based on the sublimation of materials from the heated source to the substrate located at a distance of 1-5 mm. During the CSS process both substrate and source material is heated to specific temperatures in the range of 200 °C to 700 °C under either vacuum or controlled gaseous environment (argon, nitrogen, hydrogen) [21][22].

CSS is a process that is extensively studied with a distinct influence of CdTe as the most common targeted material. Deposition can be controlled in several ways, distance to the substrate has an exponential influence on the growth rate, while changing the gaseous environment or substrate/source temperature can yield different properties of the material [23][24]. An early-stage growth mechanism has the following chain reaction: island growth (Volmer–Weber) with subsequent increase in size and density, coalescence of neighbouring islands, formation of channels and secondary nucleation [25]. Thus, the deposition should follow all mentioned stages at specific locations for the formation of high-quality materials.

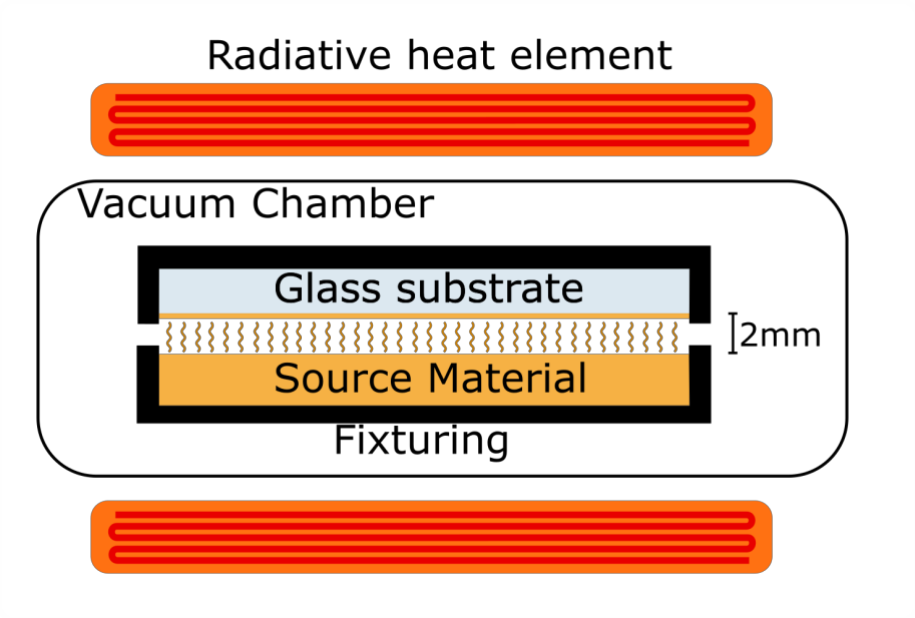

Figure 1.3 CSS reactor scheme representation [26]

Magnetron sputtering is a second widespread method of obtaining Sb_2Se_3 thin films. This technique allows for fabricating high-quality thin films by transferring material from a cathode target to an anode substrate due to ionised gas target bombardment and the subsequently directed flow of atoms in an electric field. Deposition can be performed in different gaseous environments, at different pressure, power and distance to the substrate. The co-sputtering system utilizes the setup containing several target materials at the same time, allowing the depositing of more complex materials [27]. Sputtering is a fast, scalable and reliable method to deposit thin films [28]. Figure 1.4 shows the setup for the radiofrequency (RF) magnetron sputtering system, which uses high-frequency voltage to ionise the gas in the vacuum chamber [29][30].

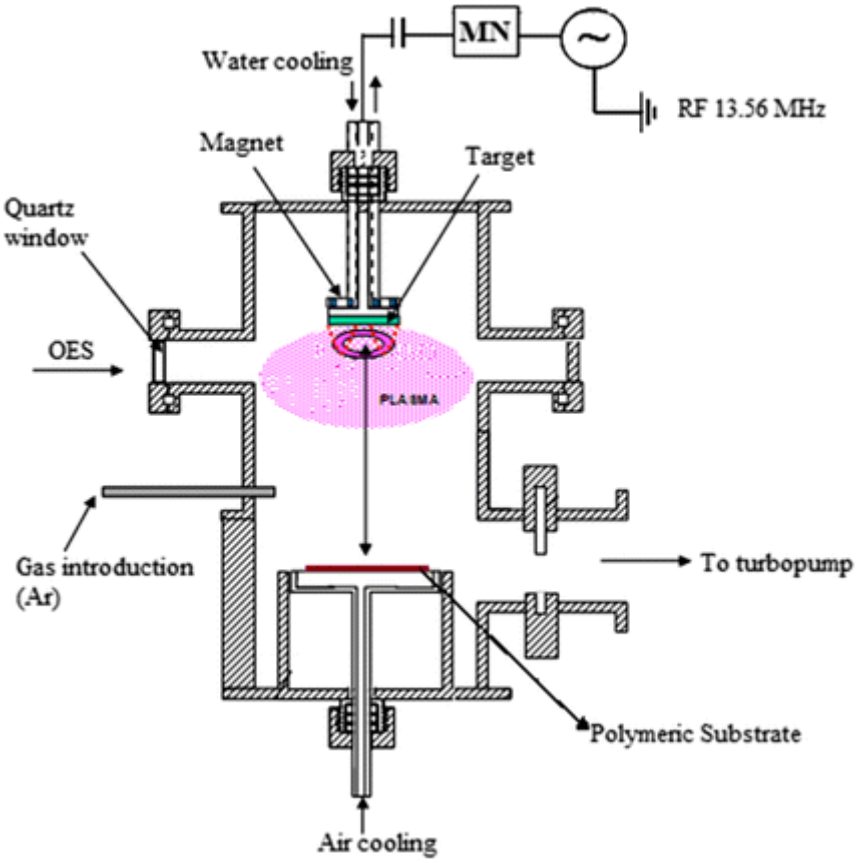

Figure 1.4 Typical RF magnetron sputtering setup [30]

In general, Sb_2Se_3 films may exhibit poor crystallinity when films are deposited by physical methods at low deposition temperatures (below 250 °C) [31][32][33]. Increasing the deposition temperature to above 300°C leads to more crystalline materials. However, Sb_2Se_3 are often contaminated by secondary phases [34][31][32][33] due to the possible decomposition according to reaction 1.1 [35]:

$$Sb_2Se_3(s) = Sb_4(g) + SbSe(g) + Se_2(g) \qquad (1.1)$$

Partial decomposition generates the conditions for forming numerous defective states in Sb_2Se_3 matrices, requiring subsequent post-deposition treatment to eliminate or passivate them.

1.2.2 Chemical deposition methods

Chemical bath deposition (CBD) uses aqueous precursor solutions and the process of obtaining the targeted thin film material usually happens due to homogeneous nucleation on the solid substrate. The main cluster of materials obtained from CBD are chalcogenides with the possibility of obtaining other films, e.g. ionic compounds [36].

CBD reaction takes place at rather low temperatures <80 °C and any non-soluble surface is suitable for deposition [37]. Figure 1.5 shows a simple setup in use for CBD, consisting of a vessel with reacting solution, submerged substrate, stirrer, a water bath surrounding a vessel placed on a heater with a magnet for the stirrer and control devices like pH meter and thermometer [37].

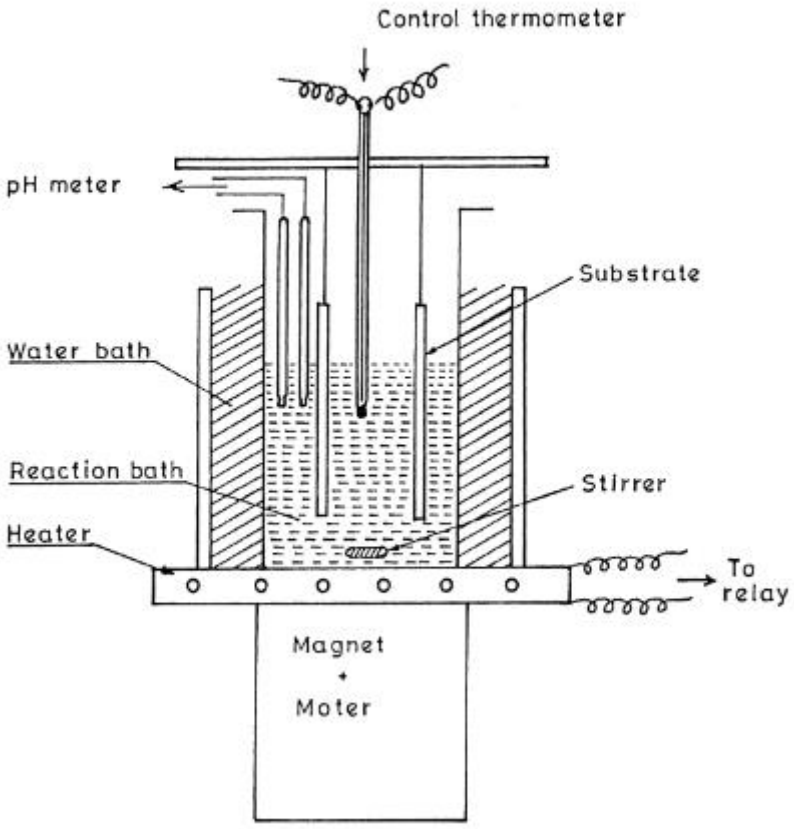

Figure 1.5 Typical CBD setup [37]

The stages of film growth in the CBD process are the following:

- monolayer formation on the surfaces due to the establishment of chemical equilibria,
- condensation of metal and chalcogen ions on the established surface,
- growth termination after reaching a peak thickness [38]

The main benefits of using CBD are simplicity, cost efficiency and scalability. A 10.57% efficient antimony selenide solar cell has been recently demonstrated using a CBD-grown absorber layer [9]. Such remarkable efficiency highlights the big potential of chemical methods to create high-quality materials.

Chemical spray pyrolysis (CSP) is a simple, scalable, and low-cost method to deposit thin films. In CSP, a precursor solution containing starting chemicals is sprayed onto

preheated substrates with the help of carrier gas. After reaching the surface, the precursor components are decomposed, forming desired films on the substrate [39]. Figure 1.6 shows a setup that can be used to deposit a film via the CSP method [40].

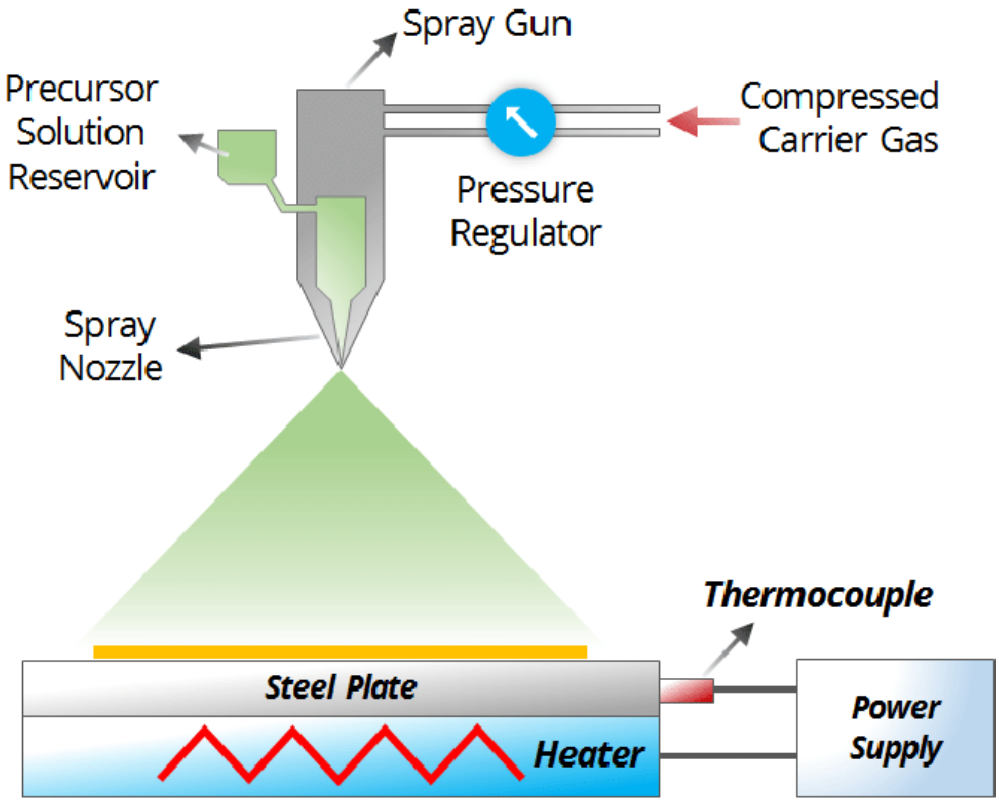

Figure 1.6 Typical CSP setup [40] *[Park]*

Even though chemical approaches to producing materials may be relatively simple, they can often lead to the contamination of the resulting materials with precursor-derived fragments and/or oxygen [9][41][42][43][44]. Eliminate these imperfections requires further post-deposition treatments or the introduction of dopants that can compensate for detrimental effects.

1.2.3 Intrinsic defects in Sb_2Se_3

Defect engineering can be crucial for Sb_2Se_3 properties as the main feature of the material: quasi-one-dimensional ribbon-like structure is prone to a more complicated defect structure than usually expected of a semiconductor consisting of two atoms [45][11]. Such materials are expected to be mainly influenced by single point defect of each type per atom, there are three types of these defects: vacancies (e.g. V_{Sb}, V_{Se}), interstitial (e.g. Sb_i, Se_i) and substitutional (e.g. Sb_{Se}, Se_{Sb}). As the symmetry of $[Sb_4Se_6]$ ribbons is low, two identical defects on Sb or Se sites can have a different influence on the structure, there are two non-equivalent atomic positions for Sb and

three for Se. This effect increases the number of actual possibilities for deviation in properties due to any of mentioned defect types in different non-equivalent sites [45][11] . An isolated [Sb_4Se_6] is shown in *Fig. 1.7* and different positions of Sb and Se are shown with different index numbers.

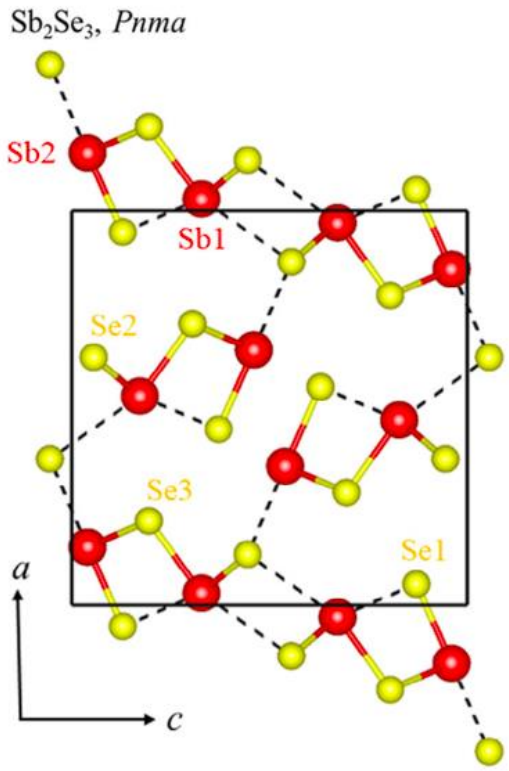

Figure 1.7 [Sb_4Se_6]$_n$ chains and non-equivalent atomic sites of Sb and Se [46]

Another unfortunate feature that comes with the ribbon-like structure is relatively large spaces between Van der Waals bonded individual ribbons, which are responsible for increased probability of substitutional defect formation or even two anions-one cation replacement ($2Se_{Sb}$), leading to the creation of highly unfavourable recombination centres [18][45][11]. An example of a Sb_{Se} substitutional defect is experimentally shown by Lian et al. in an Sb-rich structure as predicted by Huang et al. [47][45]. Quasi-1D structure is rare among other materials and thus, substitutional defects are more common in Sb_2Se_3 compared to its alternatives; thus, practical defect engineering becomes much more complicated.

1.2.4 Doping of Sb_2Se_3

Electrical, optical and structural properties of the material can be improved using various physical or chemical treatments. Apart from them, introducing foreign atoms - external doping is an additional way to manipulate the materials' properties. Energy levels that belong to introduced impurity atoms located in the shallow regions or other words,

closer to valence or conduction band are called shallow acceptors and shallow donors respectively, acceptors are favourable for p-type conductivity, while donors - for n-type. In the lattice dopants can occupy a space in between the sites of the host atoms (interstitial), the sites of atoms (substitutional), grain boundaries (GBs) or the surface, depending on the size and charge of the dopant and structure of the bulk. The main goal of introducing dopants can lay in increasing carrier density or changing the carrier type of the bulk, however, it can also change the state of intrinsic defects and introduce new ones [17].

In general, efficient p- and n-type doping can improve the electrical properties of antimony selenide. However, stabilizing p-type conductivity for Sb_2Se_3 is a very complex task, since the formation of deep-level defects such as most typical V_{Sb} and Se_{Sb} is more favourable, resulting in n-type conductivity [45][17].

Different approaches to dope Sb_2Se_3 have been reported [48][49][50]. The introduction of tellurium into thin film has shown an effect on tuning the Sb to Se ratio, which in turn slightly suppresses Se_{Sb} and V_{Sb} defects of the material grown at Se-rich conditions. Optical measurement showed no influence on the band gap, in up to 4 at% Te incorporation, presumably due to the formation of Sb_2Te_3-doped Sb_2Se_3 [51]. Tin was reported to slightly decrease the band gap from 1.17 to 1.10 in comparison to the pristine sample [52]. Another report on Sn and I doping by incorporating dopants into the magnetron sputtering target with subsequent selenization, has shown a desired band gap of ~1.1 for 1 wt% and 5 wt% -Sn and -I doped samples accordingly. A p-type conductivity of Sn doped sample and a slight stability increase in n-type conductivity with I doped one was reached [53]. The incorporation of Cu has shown GB defect passivation via $CuCl_2$ treatment [50]. Additionally, antimony selenide was reported to show n-type conductivity via the incorporation of Cl into the lattice [54]. Sodium incorporation was shown to have no impact on the electrical properties of Sb_2Se_3 [55].

Other dopants such as Te, Co, Mg, Fe, Pb, Sn, I have been tested to incorporate into antimony selenide via sputtering, solution treatment, electrodeposition, vapour transport deposition, and thermal evaporation [48][56-63].

1.3 Applications of Sb_2Se_3

The most well-researched application for antimony selenide lies in thin-film solar cells, which is a mature technology for photovoltaic devices. Thin-film solar cells typically consist of multilayered materials with thicknesses ranging from a few nanometers to hundreds of micrometres deposited on plastic, glass, or conductive oxide substrates. Cadmium telluride (CdTe) has been a successfully industrialized and commercialized material for thin-film PVs, but its toxicity has been a concern for a long time, leading to the emergence of alternative materials.
Antimony selenide is a less-toxic chalcogenide material that has emerged as a promising alternative for thin-film PVs. Along with other materials like tin sulfide, bismuth sulfide, etc., antimony selenide has demonstrated a champion efficiency of around 10% within one decade [12].

Table 1.1 Sb_2Se_3 properties comparison to CdTe

	Sb_2Se_3	**CdTe**	Ref.
Melting point [K]	885	1314	[64][65]
Band gap [eV]	1.03 (direct) 1.17 (indirect)	1.5	[64][65]
Absorption coefficient [cm^{-1}]	$>10^5$	10^4	[64][65]
Relative dielectric constant [ε_0]	15.1	10.2	[64][65]
Mobility [$cm^2\ V^{-1}\ s^{-1}$]	$\mu_e = 15$, $\mu_h = 42$	$\mu_e = 700$, $\mu_h = 65$	[64][65]
Free carrier concentration [cm^{-3}]	$\sim10^{13}$	$\sim10^{16}$	[66][67]

As illustrated in *Table 1.1*, antimony selenide has several superior properties compared to CdTe, absorption coefficient, dielectric constant and in particular lower melting point which decreases the demand for energy use during fabrication. On the other side, a main holding factor of the material is also apparent - relatively poor electrical properties.

State-of-the-art Sb_2Se_3 thin film solar cells mainly utilise CdS, ZnO or TiO_2 as buffer layers [68][69][70], one of the alternative pathways can be quasi-homojunction solar cells, limiting issues associated with band misalignment and interface recombination. Only a few studies on this topic have been made, with doping by Cu and/or I proposed

to create a quasi-homojunction of two separately deposited antimony selenide layers. Magnetron sputtering used for doping in this context requires additional heat treatment and it was noted that dopants like I inhibit large grain formation, thus limiting the quality of n-type film via the proposed method. Despite the limitations mentioned, >2% efficiencies from three reports to date show potential in this area [57][71][53].

Another important application of Sb_2Se_3 thin films is photoelectrochemical water splitting (PEC), which uses solar energy to induce the formation of H_2 and O_2 in the aqueous electrolyte – solar-to-hydrogen (STH) process. A water-splitting device can consist of a single anode - an n-type semiconductor and Pt electrode, a single cathode - a p-type semiconductor and Pt electrode, or tandem, using both n and p-type materials as photoanodes and photocathodes respectively [72]. Antimony selenide is studied as a p-type absorber for photocathodes, as competitive current density reaching as high as 30 mA cm^2, relative stability in operation and onset potential of ~0.6 V_{RHE} in combination with low toxicity, low cost of raw materials and deposition, highlight the potential in the area [71]. Recent breakthrough, exceeding the 10% efficiency barrier with Sb_2Se_3-perovskite tandem device and 3% half-cell efficiencies reported on antimony selenide photocathodes only, reflects the dynamic nature of development in the area (Figure 1.8) [73][74].

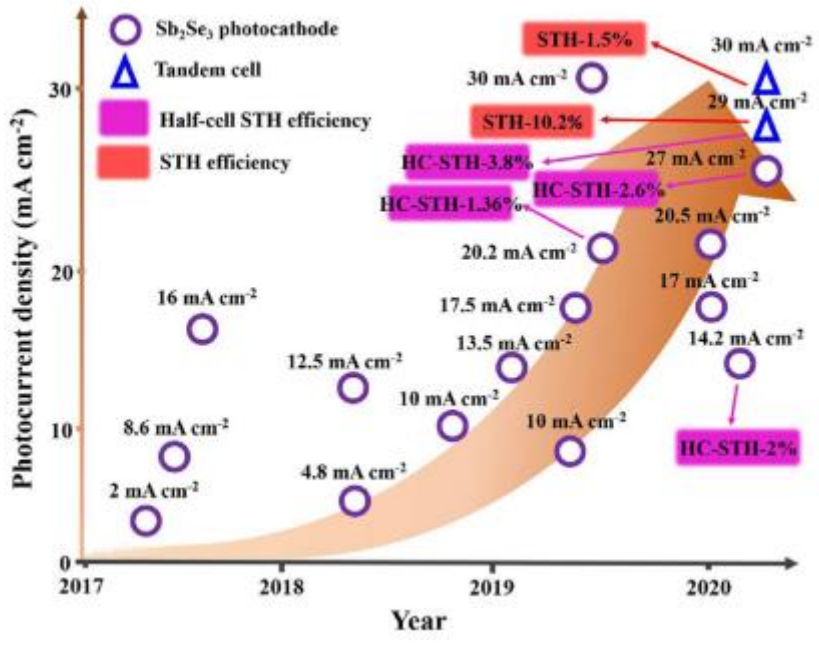

Figure 1.8 Recent developments in Sb_2Se_3 PEC devices. STH - solar-to-hydrogen conversion efficiency (total efficiency of the device), HC-STH - half cell solar-to-hydrogen efficiency (efficiency of only Sb_2Se_3 cathode) [71]

Similarly to thin film solar cells, absorber layer engineering plays a crucial role in delivering high-efficiency devices. Thus, ensuring high crystallinity and grain orientation

combined with low deep defect concentration and a need for better electrical properties can be approached by careful selection of deposition methods in combination with p-type doping [12][71]. Key aspects of the PEC device engineering for ensuring high efficiencies are shown in Figure *1.9*.

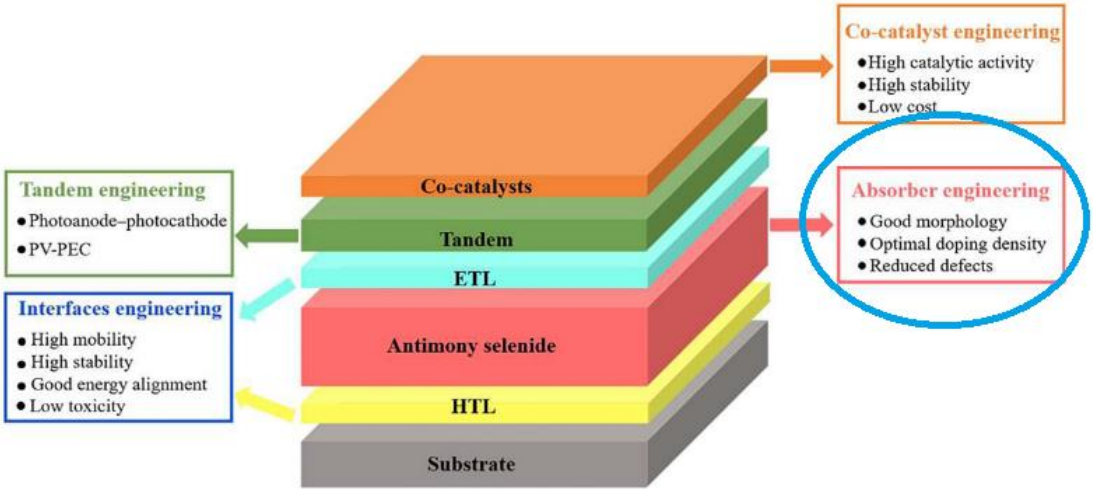

Figure 1.9 PEC device engineering pathways for improving efficiency by Chen et al. [71]

To summarize, the typical deposition methods for producing antimony selenide thin films have limitations in controlling secondary phases and approaching desired optoelectronic properties. To improve the optoelectronic properties of Sb_2Se_3 layers, various post-deposition thermal or chemical treatments, including different doping options, are typically employed. Most doping approaches listed above have demonstrated minimal success. Therefore, additional efforts need to be developed for producing efficient optoelectronic devices.

1.4 Ion Exchange

Ion exchange can be a very powerful technique to tune the materials' properties.
Both anion and cation exchange reactions (AER/CER) have been tested for optimizing or developing new features. Most of the research is focused on the transformation and doping of nanostructures and nanoparticles, rather than the development of efficient thin films. In general, ion exchange reactions based on replacing anions are less investigated due to the larger sizes of anions compared to cations and thus lower mobilities, longer reaction time and higher temperatures [75].
Straightforward techniques of chemical material synthesis of either thin film on the substrate or colloidal nanocrystals are influenced by several factors such as nucleation, surface ligation, and growth kinetics, limiting the control over the overall structure and composition. It represents a critical limitation when a complex structure or composition is desired. CERs on the contrary can take advantage of the host lattice, unlocking an

opportunity to combine a well-defined composition and morphology with the metastability of the final product [76]. Two main factors influence the exchange reaction: thermodynamics and kinetics.

Main Principles

The direction of the reaction can be predicted by combining formation energies (ΔG_{f0}) and electrode potentials (E) of all the reactants and products, subsequently calculating the Gibbs free energy of the whole reaction (ΔG_f) [77]. CER for the isovalent ions can be expressed in the following way:

$$AX\ (s)\ +\ B^{n+}(sol)\ \rightarrow\ BX\ (s)\ +\ A^{n+}(sol), \qquad (1.2)$$

where *AX* is a solid ionic crystal exposed to B^{n+} cations in the solution, producing *BX* ionic crystal and releasing A^{n+} cations into the solution (non-isovalent systems are also possible, a monovalent one was chosen for simplicity). This reaction can be broken down in the following way:

$$1)\ AX\ \rightarrow A\ +\ X\ \ (dissociation), \qquad (1.3)$$

$$2)\ B^{n+}\ \rightarrow B\ (desolvation), \qquad (1.4)$$

$$3)\ B\ +\ X\ \rightarrow BX\ \ (association), \qquad (1.5)$$

$$4)\ A\ \rightarrow A^{n+}(solvation), \qquad (1.6)$$

Calculated energies can be related to crystal strength and solvation. Equations (1.3) and (1.5) describe crystal strength: Born-Lande derived crystal energy and surface energy. Additional lattice energies can also influence the thermodynamics of the reaction, mainly due to strain and dislocation. Solvation-related energies are describing the rate at which a cation is tending to associate/dissociate to/from the lattice, eq. (1.4), (1.6). It is preferred for the parent cation to be more solvated than the desired ion. In some reactions relative lattice energy difference can be the driving factor determining the outcome. Gibbs free energy of the whole reaction, by Hess's law [77]:

$$\Delta G_f\ =\ -n\Delta G_{f0}\ (BX)\ -n\Delta G_{f0}\ (AX)\ +\ F(nE^{0}_{B^{n+}/B} - nE^{0}_{A^{n+}/A}) \qquad (1.7)$$

Where E^0 - is the standard redox potential, ΔG_{f0}- individual Gibb's energy of formation, ΔG_f- Gibb's energy of the reaction.

Kinetics

As mentioned before, adequate solvation and desolvation of ions are crucial for the CER, luckily there is a way to influence these properties of the reaction by introducing

different solvents and ligands. Hard and soft Lewis acids and bases theory is a powerful practical tool for predicting the stability and reaction mechanism of metal-ligand pairs and it has a particular application in cation exchange for ensuring higher relative solvation of ion A^{n+} compared to the target ion B^{n+}.

The presence of activation energy barriers or the limited ability of targeted ions to diffuse into the lattice is a major limiting factor in CER even in favourable thermodynamic conditions. Thus, it is critical to acknowledge the sizes of ions and host lattice parameters in the context of a particular reaction. The lattice diffusivity can define whether the reaction will take place only on the surface or the deeper penetration will be possible. In the latter reaction stage, cation exchange can lead to the formation of new phases starting at an energetically favourable nucleation point with subsequent "kicking out" of the host ions [78].

1.5 Summary and aims of the thesis

Antimony selenide thin films have high potential in various applications and are already quite extensively studied specifically in the context of solar cell devices. However, the synthesis of a high-quality film is not a trivial task due to the complex defect structure [11] and the limitations of established methods.

The Stoichiometric Sb-Se ratio is a key to low defect concentration [11], at the same time physically deposited films struggle from either low crystallinity (at lower temperatures) or undesirable phases (at higher temperatures) while chemically deposited ones are often contaminated or develop an oxide phase. In both cases, control over the phase composition and defect structure determines the potential applicability of formed materials. Improving the optoelectronic properties can be realized using various post-deposition treatments or introducing dopants.

Different attempts to stabilize the conductivity type and passivate defects presented in antimony selenide have been reported in the literature. Numerous elements including doping with Te, Cu, Co, Mg, Fe, Pb, Sn, I, Cl have been tested to stabilize the conductivity type or passivate the defects in antimony selenide films. Most reports have demonstrated minimal success.

Ion exchange is a low-cost and scalable technique that can be used for synthesizing complex nanoscale structures. Its potential to fabricate efficient thin films or introduce dopants is unclear at the current stage. Up to now, there have been no reports covering the development of doping approaches for thin films using cation exchange as a tool.

Therefore, this thesis aims to check the applicability of cation exchange to incorporate silver into antimony selenide thin films at the doping level.

2. EXPERIMENTAL SECTION

2.1 Synthesis of Sb_2Se_3 films

Antimony (III) selenide thin films were obtained by transforming sputtered SnSe into Sb_2Se_3 thin films. A radiofrequency (RF) magnetron sputtering system, Evovac 030 (Angstrom Engineering, Kitchener, ON, Canada) was used to deposit tin (II) selenide thin film onto Mo and FTO substrates. A 4-inch commercially available SnSe target (4N, LOT: PLA546838312, Plasmaterials, Inc., Livermore, CA, USA) was situated at a distance of 20 cm from the substrate holder, while the environment was held at 300 ^oC, 103 torr argon pressure and a plasma power of 88W. Obtained films were cooled to room temperature for 2 hours inside the sputtering chamber and had a thickness of around 700 nm.

SnSe films were submerged in a glycerol solution containing 44 mM of antimony chloride ($SbCl_3$) for 17 minutes at 210 ^oC. Obtained Sb_2Se_3 thin films were rinsed in deionised water and dried under the airflow.

2.2 Ag doping

Silver atoms were incorporated via a cation exchange reaction, held in Ag-rich glycerol solutions in the open environment. Two solutions were prepared, for the first one, silver source ($AgNO_3$) was mixed and completely dissolved in glycerol until the concentration reached 0.224 mM, following the addition of $NaHCO_3$ until reaching 2 mM. The second solution was prepared by simply dissolving $AgNO_3$ in desired 0.224 mM concentration. The reaction took 90 minutes at 210 ^oC after the addition of Sb_2Se_3 samples, following washing and drying in airflow.

2.3 Film Characterization

2.3.1 Scanning Electron Microscopy and Energy Dispersive X-Ray Analysis

For surface morphologies, cross-section and elemental composition a Zeiss Merlin scanning electron microscope with the Bruker EDX-XFlash6/30 detector was used at 3 kV and 20 kV acceleration voltages, for scanning electron microscopy (SEM) and energy-dispersive X-ray (EDX) measurements, respectively. Additionally, standardless analysis with the P/B-ZAF method was used for the quantitative study.

To study the surface of interest an electron beam is directed and focused on the sample. The signals that can be collected come from secondary electrons (SE), backscattered

electrons, and X-Rays. SEs are created by inelastic electron collisions, backscattered by inelastic collisions, and X-rays by exciting and relaxing atoms' electrons on the outer shell. For visualising and studying the morphology of the samples SEs are collected, while backscattered electrons can show the contrast in densities and surface roughness in the same region. X-rays, however, give information about the specific elements in the studied region, as the signal can quantify the energy level difference between the excited and relaxed state for specific elements [79][80].

2.3.2 Raman Spectroscopy

A room temperature Raman shift in the range of 50 to 600 cm^{-1} was obtained from Horiba's LabRam HR800 spectrometer (Oberursel, Germany) with a 532 nm Ar-ion laser beam and a hole diameter of 100 μm.

When a material is illuminated with light, it produces a small signal coming from normal Stokes Raman scattering due to an inelastic nature of photon collision; the incident photon energy is not equal to its energy after the collision. Thus, Raman spectroscopy can give information about the vibration of chemical bonds present in the sample [81][82]. Peaks located at different wavelengths of the incident light (laser) correspond to vibrations of specific bonds and can be studied by comparing with results from the literature.

2.3.3 X-ray Diffraction Analysis

Using a high-resolution diffractometer (Rigaku Ultima IV, Neu-Isenburg, Germany) with Cu Kα1, λ = 1.5406 Å radiation at 40 kV and 40 mA, equipped with a D/teX Ultra silicon strip detector, the structure of the samples was studied. Diffractograms of the samples were collected in a 2θ range of 10–70° with a scan step of 0.02°.

XRD utilises the diffraction phenomena that occur as the X-Ray beam is passing through a region in the sample that has a high level of order in terms of space between the atoms - crystallinity. Bragg's law (Eq. 2.1) relates the incident angle of an X-Ray beam and the distance between two successive crystal planes to the constructive interference [83][84].

$$n\lambda = 2d_{hkl}sin\theta_B, \qquad (2.1)$$

Where n is an integer, λ - wavelength of an X-ray, d_{hkl} - plane spacing, θ_B- is the angle between the incident beam and crystal plane.

Information collected from the sample via XRD is called diffractogram, which has an incident angle of the X-Ray beam on the x-axis and intensity on the y-axis, showing peaks corresponding to crystals of different orientations [83].

Crystallite size can be determined using the following relation [85]:

$$L = \frac{K\lambda}{\beta cos\theta_B} \quad (2.2)$$

Where L - crystallite size, β - width of peak's half maximum in radians.

Lattice constants of Sb_2Se_3 can be calculated in the following way:

$$\frac{1}{d_{hkl}^2} = \frac{h^2}{a^2} + \frac{k^2}{b^2} + \frac{l^2}{c^2} \quad (2.3)$$

Where h, k, l - Miller indices.

2.3.4 Photoluminescence spectroscopy

Photoluminescence (PL) spectra were obtained with a 442 nm He-Cd laser, a monochromator with a 0.64 m focal length and a single grating of 600 mm^{-1}. Temperature-dependent spectra were obtained by mounting samples onto a cold finger in a closed cycle helium cryostat (Janis CHI4, Lake Shore Cryotronics) and exciting photoluminescence at the temperature of ~8 K and gradually heating to 300 K.

Photoluminescence spectroscopy (PL) is a non-destructive and highly sensitive method of material characterization often used for determining electronic structure, defects and phases present in semiconductors. The core principle of this technique lies in the luminescence of the semiconducting material under light of a specific wavelength. As energy carried by the laser exceeds the band gap of the sample, an electron jumps to the conduction band, creating an electron-hole pair with the valence band. An electron relaxes to the conduction band minimum, losing some of its energy in the process and then finally falls back to the valence band maximum, emitting photons. Thus, electron-hole recombination can be observed, and the energy values can give an insight into the mechanism behind it [86].

Studying defects of the material can be complex as many factors have to be taken into consideration, temperature dependent measurement has to be done to analyse the dynamics of peaks shift, same as their correlation to band gap energy and often laser power too.

2.3.5 Transmission electron microscopy

Transmission electron microscopy (TEM) was used to study the incorporation of a dopant into the lattice of the base material. The TEM study was carried out using a JEOL JEM-2200FS microscope operated at 200 kV and 8–15 μA for obtaining the STEM images and EDX elemental mapping. Cross-sectional samples with a thickness of 80–100 nm were prepared using focused ion beam (FEI Helios 600 DualBeam SEM/FIB) etching.

TEM allows the study of ultra-thin samples by passing an electron beam through atoms and collecting signals as electrons that have successfully reached the detector, transmitted electrons. A simplified TEM setup consists of an electron gun, condenser, sample holder, objective, projector and detector. As electrons have to be able to pass through the sample and a high vacuum is used in the process, sample preparation is very important. Solid samples are usually cut into ~100 nm thick slices and are often treated with ionised gas to ensure the cleanliness of the surface. As electrons pass through the sample, similarly to SEM, elastically and inelastically scattered electrons can be detected, however in TEM, unscattered electrons are also used for image creation. As parallel beams penetrate the surface, an image can be obtained in two modes, by either collecting signals from unscattered or scattered electrons, called dark-field and light-field imaging, respectively [87]. Additionally, by using different lens settings, diffraction patterns can be obtained. TEM is capable of imaging the finest details, however, atomic resolution can only be achieved with materials of very low thickness, high crystallinity and relatively simple phase contrast. Scanning transmission electron microscopy (STEM) is another way of approaching imaging via TEM. In contrast to parallel electron beams directed perpendicularly to the whole sample surface during regular imaging, a focused electron beam is "scanning" the sample in STEM. As the focused beam moves through the sample, signals from inelastically scattered electrons are collected as a function of beam position and the image is recreated. EDX analysis and mapping can also be done using the TEM system in the same way as via SEM [88].

2.3.6 Ultraviolet–visible-Near Infrared spectroscopy

Optical properties were measured at room temperature in 300–1500 nm spectrum with the Cary 5000 UV-Vis-NIR spectrophotometer (Agilent Technologies, Inc., Santa Clara, CA, USA), and the band gaps of the materials were estimated using Tauc relation.

Incident light in UV, visible and NIR spectra can be transmitted, absorbed or reflected. By collecting all of the light that is transmitted or reflected, the absorption of the

material can be estimated [89][90]. Equations 3.4 and 3.5 show the relationship between the absorption coefficient, transmittance and reflectance of the sample.

$$T \approx (1 - R)^2 e^{-\alpha d} \quad (2.4)$$

$$\alpha = -\frac{1}{d} ln\left(\frac{T}{(1 - R)^2}\right) \quad (2.5)$$

Where T is transmitted light, R - is reflected light, d - thickness of a film, α - absorbance coefficient [90].

A light source is shining on the sample and slowly changing the wavelength through the whole UV-vis-NIR spectra, thus giving a possibility to relate absorption to the energy levels. Equations 3.4 and 3.5 show the relation of the band gap to absorbance for direct and indirect band structures accordingly.

$$\alpha = \frac{C(\hbar\omega - E_g)^{\frac{1}{2}}}{\hbar\omega} \quad (2.6)$$

$$\alpha = \frac{A(\hbar\omega - E_g)^2}{\hbar\omega} \quad (2.7)$$

Where E_g - band gap, ω - wavelength, $\hbar$ is Planck's constant, $and\ A$ and C are wavelength-independent constants [90].

3. RESULTS AND DISCUSSION

In stoichiometric materials, external thermodynamic driving forces are required for adequate cation replacement. It was demonstrated that monovalent activations by H, Cl, and OH of sulfide (selenide) matrices introduce numerous charge-compensating metal site vacancies, facilitating intercalation/de-intercalation of foreign ions [91][92]. Considering this, we prepared non-stoichiometric Sb_2Se_3 samples using a SnSe-to-Sb_2Se_3 transformation as reported in [91], followed by heat treatment in glycerol to introduce selenium vacancies. The selenium deficiency was confirmed by EDX (as depicted in Figure 3.1).

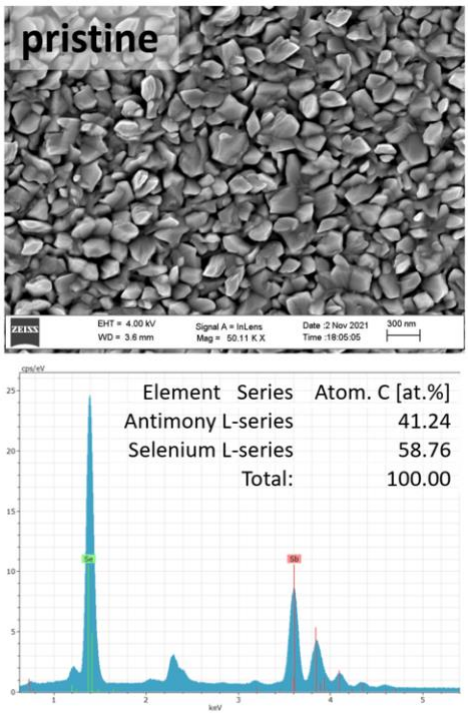

Figure 3.1 SEM surface morphology of the activated Sb_2Se_3 sample (on the top), EDX elemental composition (on the bottom)

3.1 Ag incorporation

The incorporation of monovalent silver dopants into the activated films was carried out in a glycerol solution containing $AgNO_3$. X-ray diffractometry reveals that the films being treated in a solution containing $AgNO_3$ were composed of a mixture of orthorhombic Sb_2Se_3 (ICDD database file 01-089-0821) and cubic $AgSbSe_2$ (ICDD database file 01-071-9229) phases (Figure 3.2).

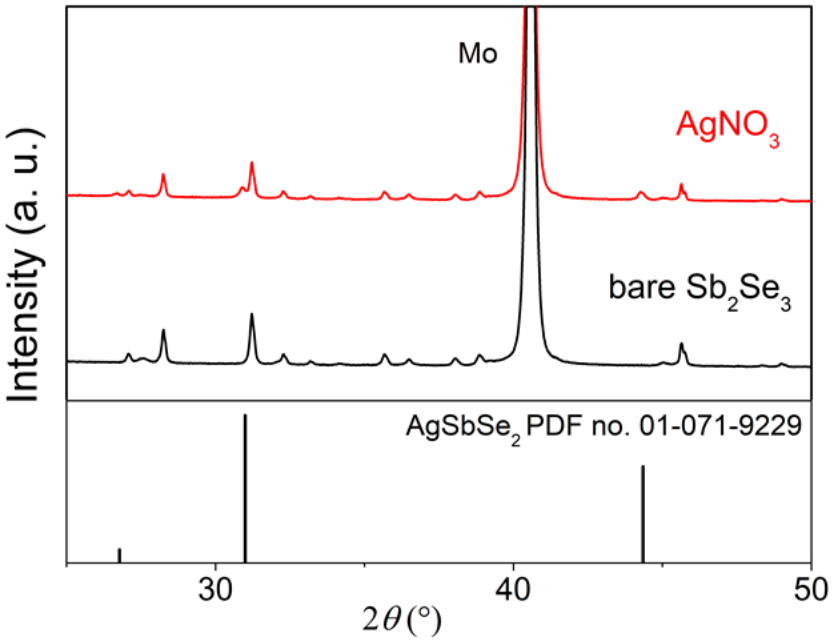

Figure 3.2 The diffractograms obtained from the sample treated in just $AgNO_3$ with $AgSbSe_2$ as a reference (PDF no. 01-071-9229)

The peak intensities of Sb_2Se_3 XRD reflections decreased significantly. This correlation accompanies a remarkable growth in the crystallite size of the $AgSbSe_2$ phase to 48 nm. Such dependence may imply a higher inversion degree of the original Sb_2Se_3 matrices.

Surface-sensitive Raman spectroscopy measurements also show a colossal difference between the crystal structures of the original and inverted samples (Fig. 3.3).

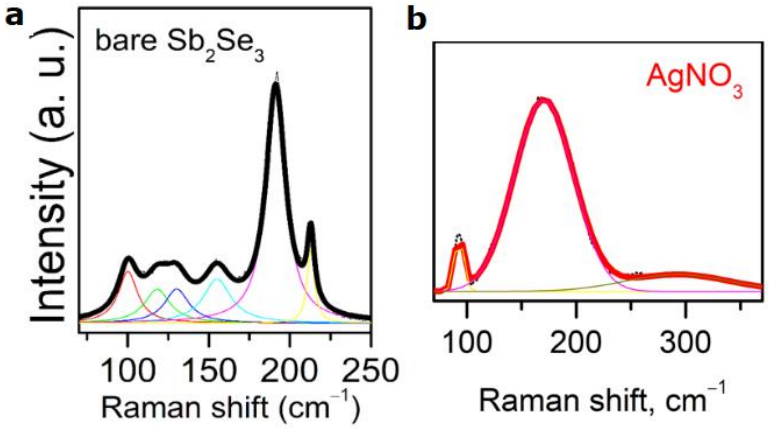

Figure 3.3 Raman spectra of (a) bare activated Sb_2Se_3 (b) Sb_2Se_3 treated in $AgNO_3$ solution

Spectroscopic assessment of the chemically silverized samples was conducted by EDX-SEM compositional analysis. According to EDX studies, the Ag content was around 10.1% in the sample treated in a solution containing $AgNO_3$ (Figure 3.4).

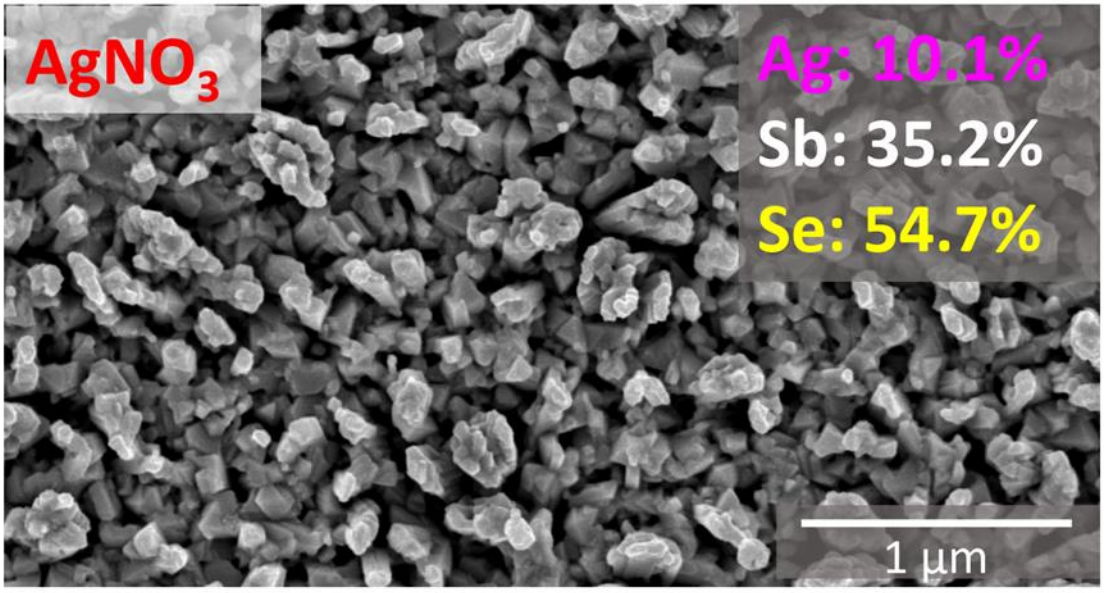

Figure 3.4 SEM/EDX surface morphology and elemental composition of the sample treated in $AgNO_3$ solution.

SEM visualization of the obtained morphology shows compliance with a polycrystalline structure and a relatively uniform grain size distribution in the 100-150 nm range. The listed above data suggest that $AgNO_3$ as a silver source when present alone in the solution initiates a notable phase transformation. To minimise a phase transition, any complexation of Ag cations is required.

Following this hypothesis, several complexing agents have been tried without any success in solution stabilizing. Only $NaHCO_3$ was capable of creating clear solutions in the presence of $AgNO_3$. Thus, $NaHCO_3$ was chosen as a complexing agent to deactivate Ag cations in the original solution. In the presence of $NaHCO_3$, Sb_2Se_3 films accumulated Ag ions at the doping levels.

3.2 Doping

Crystal structure and phases

Structural characteristics of the pristine Sb_2Se_3 and those samples treated in the Ag: NaHCO3 solution were investigated using X-ray diffractometry and Raman spectroscopy (Fig. 3.5, 3.6). Both samples exhibit diffraction patterns consistent with a single phase

of Sb_2Se_3 (ICDD database file 01-089-0821) that can be ascribed to the orthorhombic Sb_2Se_3 structure.

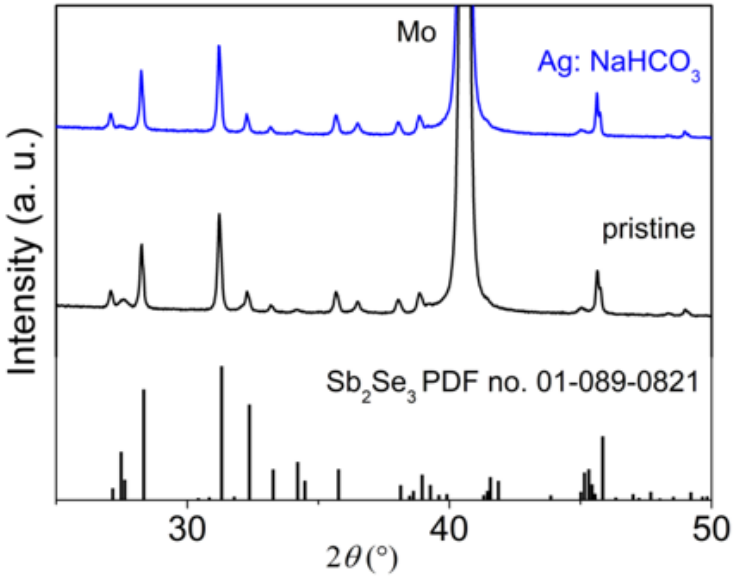

Figure 3.5 The diffractograms obtained from the sample treated in Ag:$NaHCO_3$ solution, with Sb_2Se_3 as a reference (PDF no. 01-089-0821)

Deconvoluted Raman spectra show six unaltered peak positions, evidencing no changes introduced to the crystal structure by incorporating Ag at low concentrations (Fig. 3.6).

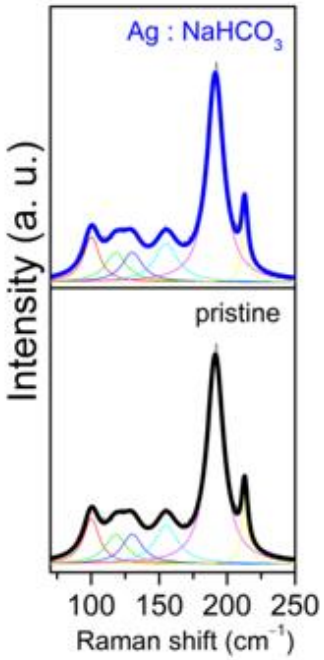

Figure 3.6 Raman spectra of Sb_2Se_3 treated in Ag: $NaHCO_3$ solution (on the top) and pre-activated Sb_2Se_3 films (on the bottom)

Elemental composition and morphology

Energy dispersive X-ray spectroscopy revealed Ag concentrations below the detection limit when using a detector integrated into a scanning electron microscope (EDX-SEM) and around 1.5 at% when using a detector in a transmission electron microscope (EDX-TEM) (Fig. 3.7).

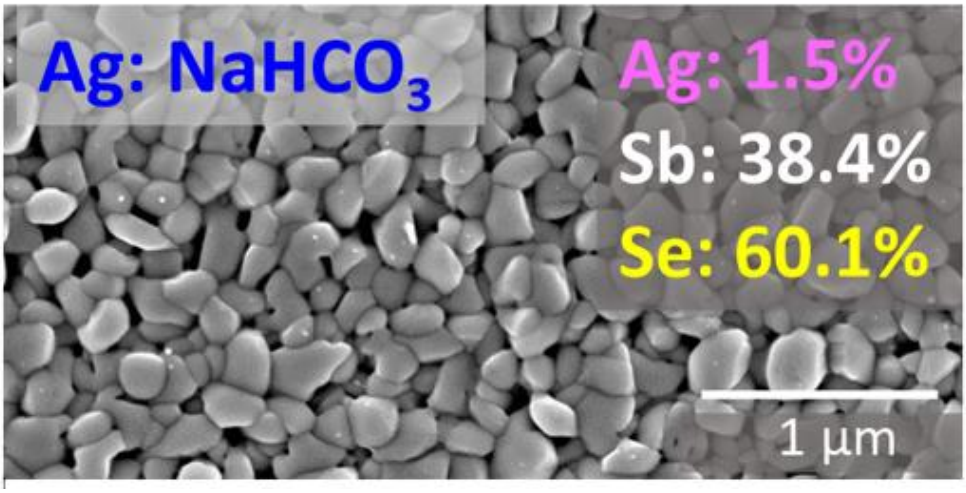

Figure 3.7 SEM surface morphology and TEM: EDX elemental composition of the sample treated in Ag: $NaHCO_3$ solution.

The cross-sectional STEM mapping shows no visible agglomerations of Ag in the Sb_2Se_3 lattice (Figure 3.8).

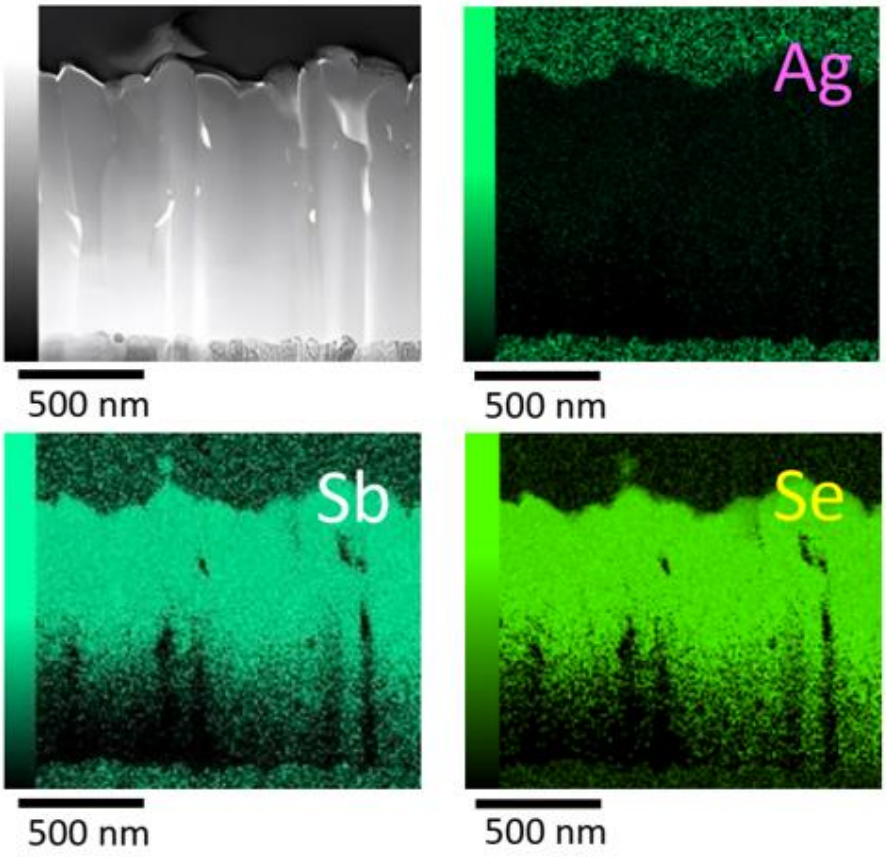

Figure 3.8 STEM cross-section image with EDX elemental mapping

Optical properties

The optical bandgap values of the pristine films and Ag-doped Sb_2Se_3 films were determined from optical transmission data using the Tauc relation (Figure 3.9). The spectra were collected using the samples grown on FTO substrates. According to the UV-Vis data, both pristine and Ag-doped Sb_2Se_3 samples demonstrate bandgap values of 1.28 eV, a typical value for the orthorhombic Sb_2Se_3 phase. Thus, the optical data agree with the data from XRD, Raman, EDX, and TEM measurements.

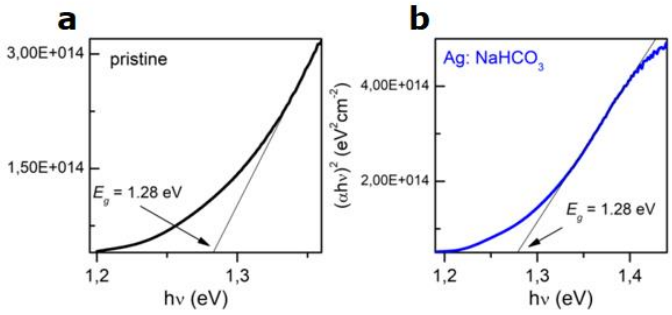

Figure 3.9 Tauc plot from UV-Vis measurement for (a) activated Sb_2Se_3 sample and (b) Sb_2Se_3 treated by a combination of $AgNO_3$ and $NaHCO_3$

PL measurements

The effects caused by incorporating Ag at doping levels were further explored using PL spectroscopy. Figures 3.10a and 3.10b show experimental low-temperature PL spectra of pristine and Ag-doped Sb_2Se_3 samples. The pristine Sb_2Se_3 film exhibits one emission peak at ~0.9 eV, presumably ascribed to a deep donor–deep acceptor (DD–DA) recombination [93]. Silver incorporation induces drastic changes in the PL data, resulting in the appearance of four distinct bands (Fig. 3.10b).

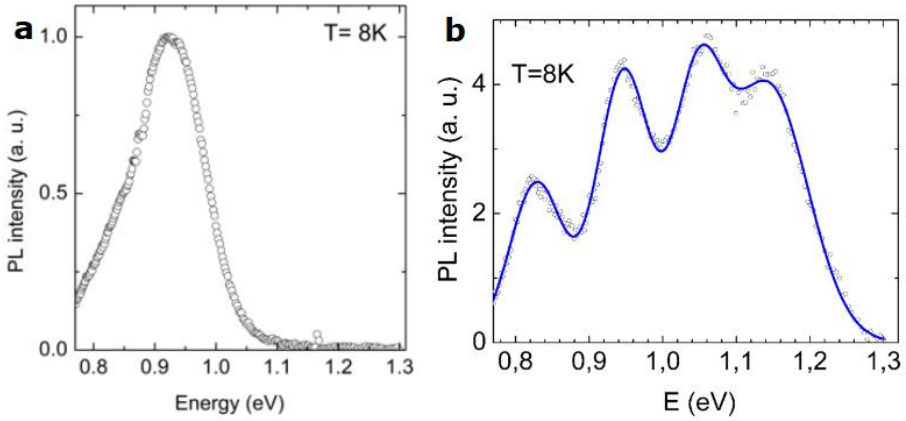

Figure 3.10 (a) low-temperature PL of pristine Sb_2Se_3 (b) low-temperature PL of doped Sb_2Se_3

The temperature dependence of these PL bands demonstrates very fast quenching without discernible alterations in the peak positions (Fig. 3.11). Such behaviour with increasing temperature predicts low thermal activation energies required for all PL bands. It could be speculated that all the observed PL bands probably originate from deep donor-deep acceptor (DD-DA) pair recombination [94][95]. A similar model was recently suggested for PL bands in polycrystalline Sb_2Se_3 [96].

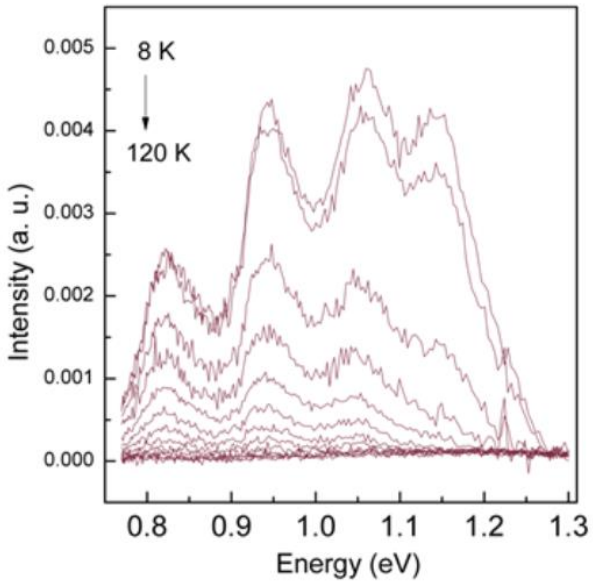

Figure 3.11 Temperature dependent PL spectra for Sb_2Se_3 films treated in a Ag: $NaHCO_3$ solution

Photoluminescence data manifested severe changes in the defect structure of Sb_2Se_3 induced by incorporating Ag at ~1.5 at%. Further studies are needed to clarify the aspects derived from Ag doping.

4. CONCLUSION

This work aimed to verify the applicability of cation exchange reactions for doping antimony (III) selenide thin films. If successful, such doping technologies can control the electrical properties of Sb_2Se_3 thin films and similar materials. Doped antimony (III) selenide can be an absorber layer for non-toxic and efficient thin-film solar cells or solar-to-hydrogen photoelectrochemical conversion devices. Various doping protocols applied to thin films represent a typical way to improve the optoelectronic properties of materials. However, to date, employing cation exchange reactions has never been reported for doping Sb_2Se_3 thin films.

In short, the main outcomes of this work can be described as follows:

1. The developed cation exchange procedures can be used to incorporate Ag atoms into Sb_2Se_3 thin films.
2. X-ray diffractometry and Raman spectroscopy revealed that $AgNO_3$ induces a severe phase transformation from the orthorhombic Sb_2Se_3 phase to the cubic $AgSbSe_2$ phase, when present alone in cation exchange solutions at concentrations of ~0.224 mM. The EDX data revealed a significant accumulation of Ag close to 10 at% in the formed Ag:Sb_2Se_3 layers.
3. The accumulation of Ag atoms in Sb_2Se_3 films can be controlled by dissolving different complexing agents in addition to a silver source.
4. Concentrations of $NaHCO_3$ in glycerol close to 2 mM are sufficient to deactivate Ag cations while keeping the solution transparent.
5. Cation exchange performed in the solution containing $AgNO_3$ at 0.224 mM and $NaHCO_3$ at 2 mM at 210 °C for 90 min leads to the incorporation of Ag into Sb_2Se_3 films at a 1.5 at%. Structural and optical properties remained unchanged after introducing Ag atoms at doping levels.
6. Silver incorporation at ~1.5 at% induces drastic changes in the PL data, resulting in the appearance of four distinct bands, different from that observed for the pristine state.

SUMMARY

The initiatives in moving away from hydrocarbon-based energy supplies call for increasing capacities of sustainable energy sources and thus materials associated with them. Solar energy is one of the most important sources of low-carbon energy and both photovoltaic solar cells and solar-to-hydrogen strategies are among highly potential tools for green energy transition. The most advanced in the commercial sense, absorber materials beyond energy-inefficient silicon are utilizing toxic and scarce materials. Antimony selenide is an emerging semiconducting material with high potential due to low toxicity, cheap raw materials, relatively energy-efficient production and suitable properties.

Antimony (III) selenide as a photovoltaic absorber layer has a near-ideal optical band gap, absorption coefficient and relative dielectric constant, while non-toxic and relatively earth-abundant elemental composition defines a potential for industrial-scale application. Various deposition methods have been tested and used consistently to produce Sb_2Se_3 thin films, however, synthesis of high-quality material using them is a nontrivial task due to factors like relatively low decomposition temperature, ease of oxygen incorporation from solvents or atmosphere and complex defect chemistry of the material itself. As a result, the optoelectronic properties are unpredictable and can yield both p- and n-type semiconductors, often not reaching desired charged carrier concentrations. Thus, due to complex defect chemistry, the progress in high-quality Sb_2Se_3 material synthesis is limited by an inability to control the optoelectronic properties.

Doping is often addressed as a way to compensate for that effect, nevertheless, multiple attempts using conventional methods have shown no significant improvement in the ability to control electrical properties and have led to the formation of undesired phases or interferences with crystal structure. Cation exchange is a technique that proved effective in doping and transformation of nanocrystals, yet not explored enough on thin films.

In this work, silver ions were introduced into Sb_2Se_3 thin films by treatment in a glycerol solution containing only $AgNO_3$ or $AgNO_3$ combined with $NaHCO_3$ at 210 ^oC for 17 minutes. It was concluded that the silver incorporation rate depends on the choice of complexing agent and in the case of pure Ag source, a partial phase transformation to $AgSbSe_2$ and Sb_2Se_3 is inevitable.

Multiple chemicals were tested to suppress phase transition and incorporate Ar ions into the lattice, yet only $NaHCO_3$ successfully suppresses Ag ions and introduces dopants without a phase change. Silver incorporation at 1.5 at% using $AgNO_3$ in combination with $NaHCO_3$ was confirmed by TEM/EDX and the phase preservation was observed by XRD and Raman spectroscopy, while PL spectroscopy showed a drastic change in comparison to the pristine sample.

LIST OF REFERENCES

[1] "The European Green Deal, COMMUNICATION FROM THE COMMISSION." https://eur-lex.europa.eu/legal-content/EN/TXT/?qid=1588580774040&uri=CELEX%3A52019DC0640 (accessed May 21, 2023).

[2] "Executive summary – World Energy Outlook 2022 – Analysis - IEA." https://www.iea.org/reports/world-energy-outlook-2022/executive-summary (accessed May 21, 2023).

[3] "Solar energy." https://energy.ec.europa.eu/topics/renewable-energy/solar-energy_en (accessed May 21, 2023).

[4] M. Nakamura, K. Yamaguchi, Y. Kimoto, Y. Yasaki, T. Kato, and H. Sugimoto, "Cd-Free Cu(In,Ga)(Se,S)2 thin-film solar cell with record efficiency of 23.35%," *IEEE J. Photovoltaics*, vol. 9, no. 6, pp. 1863–1867, Nov. 2019, doi: 10.1109/JPHOTOV.2019.2937218.

[5] "First Solar CdTe cell hits 22.1% efficiency." https://optics.org/news/7/2/29 (accessed May 21, 2023).

[6] W. Wang *et al.*, "Device Characteristics of CZTSSe Thin-Film Solar Cells with 12.6% Efficiency," *Adv. Energy Mater.*, vol. 4, no. 7, p. 1301465, May 2014, doi: 10.1002/AENM.201301465.

[7] D. M. Hart, "The Impact of China's Production Surge on Innovation in the Global Solar Photovoltaics Industry," *Inf. Technol. Innov. Found.*, no. October, pp. 2011–2013, 2020, Accessed: May 21, 2023. [Online]. Available: https://itif.org/publications/2020/10/05/impact-chinas-production-surge-innovation-global-solar-photovoltaics/.

[8] P. R. F. I. F. S. E. S. ISE, "Photovoltaics Report," no. February, 2012.

[9] Y. Zhao *et al.*, "Regulating deposition kinetics via a novel additive-assisted chemical bath deposition technology enables fabrication of 10.57%-efficiency Sb2Se3 solar cells," *Energy Environ. Sci.*, vol. 15, no. 12, pp. 5118–5128, 2022, doi: 10.1039/d2ee02261c.

[10] C. Chen, K. Li, and J. Tang, "Ten Years of Sb2Se3 Thin Film Solar Cells," *Sol. RRL*, vol. 6, no. 7, pp. 1–11, 2022, doi: 10.1002/solr.202200094.

[11] C. N. Savory and D. O. Scanlon, "The complex defect chemistry of antimony selenide," *J. Mater. Chem. A*, vol. 7, no. 17, pp. 10739–10744, 2019, doi: 10.1039/c9ta02022e.

[12] C. Chen and J. Tang, "Open-Circuit Voltage Loss of Antimony Chalcogenide Solar Cells: Status, Origin, and Possible Solutions," *ACS Energy Lett.*, vol. 5, no. 7, pp. 2294–2304, 2020, doi: 10.1021/acsenergylett.0c00940.

[13] G. Ghosh, "The sb-se (antimony-selenium) system," *J. Phase Equilibria*, vol. 14,

no. 6, pp. 753–763, 1993, doi: 10.1007/BF02667889.

[14] A. Mavlonov *et al.*, "A review of Sb2Se3 photovoltaic absorber materials and thin-film solar cells," *Sol. Energy*, vol. 201, no. February, pp. 227–246, 2020, doi: 10.1016/j.solener.2020.03.009.

[15] Mamta, Y. Singh, K. K. Maurya, and V. N. Singh, "A review on properties, applications, and deposition techniques of antimony selenide," *Sol. Energy Mater. Sol. Cells*, vol. 230, no. March, p. 111223, 2021, doi: 10.1016/j.solmat.2021.111223.

[16] V. A. Majidzade, A. S. Aliyev, I. Qasimogli, P. H. Quliyev, and D. B. Tagiyev, "Electrical Properties of Electrochemically Grown Thin Sb2Se3 Semiconductor Films," *Inorg. Mater.*, vol. 55, no. 10, pp. 979–983, 2019, doi: 10.1134/S0020168519100108.

[17] U. Wijesinghe, G. Longo, and O. S. Hutter, "Defect engineering in antimony selenide thin film solar cells," *Energy Adv.*, vol. 2, no. 1, pp. 12–33, 2023, doi: 10.1039/d2ya00232a.

[18] M. Huang, Z. Cai, S. Wang, X. G. Gong, S. H. Wei, and S. Chen, "More Se Vacancies in Sb2Se3 under Se-Rich Conditions: An Abnormal Behavior Induced by Defect-Correlation in Compensated Compound Semiconductors," *Small*, vol. 17, no. 36, pp. 1–9, 2021, doi: 10.1002/smll.202102429.

[19] T. D. C. Hobson, L. J. Phillips, O. S. Hutter, K. Durose, and J. D. Major, "Defect properties of Sb2Se3thin film solar cells and bulk crystals," *Appl. Phys. Lett.*, vol. 116, no. 26, pp. 1–6, 2020, doi: 10.1063/5.0012697.

[20] "Antimony triselenide - Wikipedia." https://en.wikipedia.org/wiki/Antimony_triselenide (accessed May 21, 2023).

[21] J. L. Ecuyer, Z. F. Tomashik, and R. Compounds, "Close Space Sublimation Crystal Growth and Surfaces," 2010.

[22] L. J. Phillips *et al.*, "Close-Spaced Sublimation for Sb2Se3Solar Cells," pp. 1445–1448, 2018, doi: 10.1109/pvsc.2017.8366746.

[23] J. L. Cruz-Campa and D. Zubia, "CdTe thin film growth model under CSS conditions," *Sol. Energy Mater. Sol. Cells*, vol. 93, no. 1, pp. 15–18, 2009, doi: 10.1016/j.solmat.2008.02.012.

[24] P. Fan *et al.*, "Quasi-Vertically Oriented Sb2Se3Thin-Film Solar Cells with Open-Circuit Voltage Exceeding 500 mV Prepared via Close-Space Sublimation and Selenization," *ACS Appl. Mater. Interfaces*, vol. 13, no. 39, pp. 46671–46680, 2021, doi: 10.1021/acsami.1c13223.

[25] J. D. Major and K. Durose, "Early stage growth mechanisms of CdTe thin films deposited by close space sublimation for solar cells," *Sol. Energy Mater. Sol. Cells*, vol. 95, no. 12, pp. 3165–3170, 2011, doi:

10.1016/j.solmat.2011.05.002.

[26] "Close-space sublimation - Wikipedia." https://en.wikipedia.org/wiki/Close-space_sublimation (accessed May 21, 2023).

[27] "What is Co-Sputtering and Co-Evaporation?" https://www.semicore.com/news/102-what-is-co-sputtering-co-evaporation (accessed May 21, 2023).

[28] S. Swann, "Magnetron sputtering," *Phys. Technol.*, vol. 19, no. 2, pp. 67–75, 1988, doi: 10.1088/0305-4624/19/2/304.

[29] "What is RF Sputtering? The Process and Applications Explained." https://korvustech.com/rf-sputtering/ (accessed May 21, 2023).

[30] S. Pedram, H. R. Mortaheb, H. Fakhouri, and F. Arefi-Khonsari, "Polytetrafluoroethylene Sputtered PES Membranes for Membrane Distillation: Influence of RF Magnetron Sputtering Conditions," *Plasma Chem. Plasma Process.*, vol. 37, no. 1, pp. 223–241, 2017, doi: 10.1007/s11090-016-9769-3.

[31] R. Tang, X. Y. Chen, G. X. Liang, Z. H. Su, J. ting Luo, and P. Fan, "Magnetron sputtering deposition and selenization of Sb 2 Se 3 thin film for substrate Sb 2 Se 3 /CdS solar cells," *Surf. Coatings Technol.*, vol. 360, no. November 2018, pp. 68–72, 2019, doi: 10.1016/j.surfcoat.2018.12.102.

[32] C. Ma *et al.*, "Fabrication of Sb2Se3 thin film solar cells by co-sputtering of Sb2Se3 and Se targets," *Sol. Energy*, vol. 193, no. September, pp. 275–282, 2019, doi: 10.1016/j.solener.2019.09.046.

[33] G. X. Liang *et al.*, "Thermally induced structural evolution and performance of Sb2Se3 films and nanorods prepared by an easy sputtering method," *Sol. Energy Mater. Sol. Cells*, vol. 174, no. December 2016, pp. 263–270, 2018, doi: 10.1016/j.solmat.2017.09.008.

[34] A. K. Jain, C. Gopalakrishnan, and P. Malar, "Study of pulsed laser deposited antimony selenide thin films," *J. Mater. Sci. Mater. Electron.*, vol. 33, no. 13, pp. 10430–10438, 2022, doi: 10.1007/s10854-022-08030-1.

[35] and A. N. G. Gospodinov, A. Pashinkin, Z. Boncheva-Mladenova, "Determination of the Saturated Vapour Pressure of Solid Antimony Selenide," *Fiz.Mater*, vol. 6, p. 726, 1970.

[36] G. Hodes, "Semiconductor and ceramic nanoparticle films deposited by chemical bath deposition," *Phys. Chem. Chem. Phys.*, vol. 9, no. 18, pp. 2181–2196, 2007, doi: 10.1039/b616684a.

[37] R. S. Mane and C. D. Lokhande, "Chemical deposition method for metal chalcogenide thin films," *Mater. Chem. Phys.*, vol. 65, no. 1, pp. 1–31, 2000, doi: 10.1016/S0254-0584(00)00217-0.

[38] P. K. Nair, P. Parmananda, and M. T. S. Nair, "Mathematical model simulating

the growth of compound semiconductor thin films via chemical bath deposition," *J. Cryst. Growth*, vol. 206, no. 1–2, pp. 68–74, 1999, doi: 10.1016/S0022-0248(99)00287-0.

[39] S. Rahemi Ardekani, A. Sabour Rouh Aghdam, M. Nazari, A. Bayat, E. Yazdani, and E. Saievar-Iranizad, "A comprehensive review on ultrasonic spray pyrolysis technique: Mechanism, main parameters and applications in condensed matter," *J. Anal. Appl. Pyrolysis*, vol. 141, no. March, p. 104631, 2019, doi: 10.1016/j.jaap.2019.104631.

[40] S. I. Park *et al.*, "A review on fabrication processes for electrochromic devices," *Int. J. Precis. Eng. Manuf. - Green Technol.*, vol. 3, no. 4, pp. 397–421, 2016, doi: 10.1007/s40684-016-0049-8.

[41] S. Messina, M. T. S. Nair, and P. K. Nair, "Antimony Selenide Absorber Thin Films in All-Chemically Deposited Solar Cells," *J. Electrochem. Soc.*, vol. 156, no. 5, p. H327, 2009, doi: 10.1149/1.3089358.

[42] Y. Rodríguez-Lazcano, Y. Peña, M. T. S. Nair, and P. K. Nair, "Polycrystalline thin films of antimony selenide via chemical bath deposition and post deposition treatments," *Thin Solid Films*, vol. 493, no. 1–2, pp. 77–82, 2005, doi: 10.1016/j.tsf.2005.07.238.

[43] K. Y. Rajpure and C. H. Bhosale, "Preparation and characterization of spray deposited photoactive Sb2S3 and Sb2Se3 thin films using aqueous and non-aqueous media," *Mater. Chem. Phys.*, vol. 73, no. 1, pp. 6–12, 2002, doi: 10.1016/S0254-0584(01)00350-9.

[44] K. Y. Rajpure and C. H. Bhosale, "Effect of Se source on properties of spray deposited Sb2Se3 thin films," *Mater. Chem. Phys.*, vol. 62, no. 2, pp. 169–174, 2000, doi: 10.1016/S0254-0584(99)00173-X.

[45] M. Huang, P. Xu, D. Han, J. Tang, and S. Chen, "Complicated and Unconventional Defect Properties of the Quasi-One-Dimensional Photovoltaic Semiconductor Sb 2 Se 3," *ACS Appl. Mater. Interfaces*, vol. 11, no. 17, pp. 15564–15572, 2019, doi: 10.1021/acsami.9b01220.

[46] M. G. Herrmann *et al.*, "Lattice Dynamics of Sb2Se3 from Inelastic Neutron and X-Ray Scattering," *Phys. Status Solidi Basic Res.*, vol. 257, no. 6, pp. 3–9, 2020, doi: 10.1002/pssb.202000063.

[47] W. Lian *et al.*, "Distinctive Deep-Level Defects in Non-Stoichiometric Sb2Se3 Photovoltaic Materials," *Adv. Sci.*, vol. 9, no. 9, pp. 1–7, 2022, doi: 10.1002/advs.202105268.

[48] D. Ren *et al.*, "Structure, morphology, and photoelectric performances of te-sb2se3 thin film prepared via magnetron sputtering," *Nanomaterials*, vol. 10, no. 7, pp. 1–13, 2020, doi: 10.3390/nano10071358.

[49] G. Spaggiari *et al.*, "Exploring Cu-Doping for Performance Improvement in Sb2Se3 Photovoltaic Solar Cells," *Int. J. Mol. Sci.*, vol. 23, no. 24, 2022, doi: 10.3390/ijms232415529.

[50] C. Chen *et al.*, "Efficiency Improvement of Sb2Se3 Solar Cells via Grain Boundary Inversion," *ACS Energy Lett.*, vol. 3, no. 10, pp. 2335–2341, 2018, doi: 10.1021/acsenergylett.8b01456.

[51] Y. Ma *et al.*, "Efficient defect passivation of Sb2Se3 film by tellurium doping for high performance solar cells," *J. Mater. Chem. A*, vol. 8, no. 14, pp. 6510–6516, 2020, doi: 10.1039/d0ta00443j.

[52] S. Chen *et al.*, "Enhanced electrical conductivity and photoconductive properties of Sn-doped Sb2Se3 crystals," *J. Mater. Chem. C*, vol. 6, no. 24, pp. 6465–6470, 2018, doi: 10.1039/c8tc01683f.

[53] G. Liang *et al.*, "Ion doping simultaneously increased the carrier density and modified the conduction type of Sb2Se3 thin films towards quasi-homojunction solar cell," *J. Mater.*, vol. 7, no. 6, pp. 1324–1334, 2021, doi: 10.1016/j.jmat.2021.02.009.

[54] T. D. C. Hobson *et al.*, "Isotype Heterojunction Solar Cells Using n-Type Sb2Se3 Thin Films," *Chem. Mater.*, vol. 32, no. 6, pp. 2621–2630, 2020, doi: 10.1021/acs.chemmater.0c00223.

[55] Y. Li *et al.*, "The effect of sodium on antimony selenide thin film solar cells," *RSC Adv.*, vol. 6, no. 90, pp. 87288–87293, 2016, doi: 10.1039/c6ra20690e.

[56] R. S. Rahman, K. Asokan, and M. Zulfequar, "Mitigation of Surface Oxidation in Sb2Se3Thin Films Via Te Doping: An Effective Strategy Towards Realization of Efficient Electronic Devices," *J. Phys. Chem. C*, vol. 126, no. 13, pp. 6065–6074, 2022, doi: 10.1021/acs.jpcc.2c00336.

[57] D. Ren, S. Chen, M. Cathelinaud, G. Liang, H. Ma, and X. Zhang, "Fundamental Physical Characterization of Sb2Se3-Based Quasi-Homojunction Thin Film Solar Cells," *ACS Appl. Mater. Interfaces*, vol. 12, no. 27, pp. 30572–30583, 2020, doi: 10.1021/acsami.0c08180.

[58] D. Sun, Y. Fang, X. Yan, W. Shan, W. Sun, and Q. Meng, "Ultrafast Broadband Nonlinear Optical Response in Co-Doped Sb2Se3 Nanofilms at Near-Infrared," *Front. Mater.*, vol. 8, no. September, pp. 1–13, 2021, doi: 10.3389/fmats.2021.721101.

[59] W. H. Li *et al.*, "Enhanced performance of antimony selenide thin film solar cell using PbI2as a dopant," *Appl. Phys. Lett.*, vol. 118, no. 9, 2021, doi: 10.1063/5.0040940.

[60] M. B. Costa, F. W. de Souza Lucas, and L. H. Mascaro, "Electrodeposition of Fe-doped Sb2Se3 thin films for photoelectrochemical applications and study of the

doping effects on their properties," *J. Solid State Electrochem.*, vol. 22, no. 5, pp. 1557–1562, 2018, doi: 10.1007/s10008-017-3768-z.

[61] Y. Li *et al.*, "Characterization of Mg and Fe doped Sb2Se3 thin films for photovoltaic application," *Appl. Phys. Lett.*, vol. 109, no. 23, pp. 1–6, 2016, doi: 10.1063/1.4971388.

[62] M. Huang *et al.*, "p-Type Antimony Selenide via Lead Doping," *Sol. RRL*, vol. 6, no. 7, pp. 1–9, 2022, doi: 10.1002/solr.202100730.

[63] T. D. C. Hobson *et al.*, "P-type conductivity in Sn-doped Sb 2 Se 3 Journal of Physics : Energy OPEN ACCESS," 2022.

[64] J. Dong, Y. Liu, Z. Wang, and Y. Zhang, " Boosting V OC of antimony chalcogenide solar cells: A review on interfaces and defects ," *Nano Sel.*, vol. 2, no. 10, pp. 1818–1848, 2021, doi: 10.1002/nano.202000288.

[65] "Cadmium Telluride (CdTe) Semiconductors." https://www.azom.com/article.aspx?ArticleID=8408 (accessed May 21, 2023).

[66] C. Chen *et al.*, "Characterization of basic physical properties of Sb2Se3 and its relevance for photovoltaics," *Front. Optoelectron.*, vol. 10, no. 1, pp. 18–30, 2017, doi: 10.1007/s12200-017-0702-z.

[67] B. E. McCandless *et al.*, "Overcoming Carrier Concentration Limits in Polycrystalline CdTe Thin Films with In Situ Doping," *Sci. Rep.*, vol. 8, no. 1, pp. 1–13, 2018, doi: 10.1038/s41598-018-32746-y.

[68] X. Wen *et al.*, "Vapor transport deposition of antimony selenide thin film solar cells with 7.6% efficiency," *Nat. Commun.*, vol. 9, no. 1, 2018, doi: 10.1038/s41467-018-04634-6.

[69] L. Wang *et al.*, "Stable 6%-efficient Sb2Se3 solar cells with a ZnO buffer layer," *Nat. Energy*, vol. 2, no. 4, pp. 1–9, 2017, doi: 10.1038/nenergy.2017.46.

[70] H. Deng *et al.*, "Efficient and stable TiO2/Sb2S3 planar solar cells from absorber crystallization and Se-atmosphere annealing," *Mater. Today Energy*, vol. 3, pp. 15–23, 2017, doi: 10.1016/j.mtener.2017.02.001.

[71] S. Chen *et al.*, "Recent progress and perspectives on Sb2Se3-based photocathodes for solar hydrogen production via photoelectrochemical water splitting," *J. Energy Chem.*, vol. 67, pp. 508–523, 2022, doi: 10.1016/j.jechem.2021.08.062.

[72] M. G. Walter *et al.*, "Solar water splitting cells," *Chem. Rev.*, vol. 110, no. 11, pp. 6446–6473, 2010, doi: 10.1021/cr1002326.

[73] W. Yang *et al.*, "Solar water splitting exceeding 10% efficiency: Via low-cost Sb2Se3photocathodes coupled with semitransparent perovskite photovoltaics," *Energy Environ. Sci.*, vol. 13, no. 11, pp. 4362–4370, 2020, doi: 10.1039/d0ee02959a.

[74] C. Liu *et al.*, "A dendritic Sb2Se3/In2S3heterojunction nanorod array photocathode decorated with a MoS: xcatalyst for efficient solar hydrogen evolution," *J. Mater. Chem. A*, vol. 8, no. 44, pp. 23385–23394, 2020, doi: 10.1039/d0ta08874a.

[75] J. B. Rivest and P. K. Jain, "Cation exchange on the nanoscale: An emerging technique for new material synthesis, device fabrication, and chemical sensing," *Chem. Soc. Rev.*, vol. 42, no. 1, pp. 89–96, 2013, doi: 10.1039/c2cs35241a.

[76] B. J. Beberwyck and A. P. Alivisatos, "Ion exchange synthesis of III-V nanocrystals," *J. Am. Chem. Soc.*, vol. 134, no. 49, pp. 19977–19980, 2012, doi: 10.1021/ja309416c.

[77] X. Li *et al.*, "Cation/Anion Exchange Reactions toward the Syntheses of Upgraded Nanostructures: Principles and Applications," *Matter*, vol. 2, no. 3, pp. 554–586, 2020, doi: 10.1016/j.matt.2019.12.024.

[78] L. De Trizio and L. Manna, "Forging colloidal nanostructures via cation exchange reactions," *Chem. Rev.*, vol. 116, no. 18, pp. 10852–10887, 2016, doi: 10.1021/acs.chemrev.5b00739.

[79] "Scanning electron microscope - Wikipedia." https://en.wikipedia.org/wiki/Scanning_electron_microscope (accessed May 21, 2023).

[80] "The Applications and Practical Uses of Scanning Electron Microscopes - ATA Scientific." https://www.atascientific.com.au/sem-imaging-applications-practical-uses-scanning-electron-microscopes/ (accessed May 21, 2023).

[81] "Raman scattering - Wikipedia." https://en.wikipedia.org/wiki/Raman_scattering (accessed May 21, 2023).

[82] "Raman spectroscopy - Wikipedia." https://en.wikipedia.org/wiki/Raman_spectroscopy (accessed May 21, 2023).

[83] G. F. Harrington and J. Santiso, "Back-to-Basics tutorial: X-ray diffraction of thin films," *J. Electroceramics*, vol. 47, no. 4, pp. 141–163, 2021, doi: 10.1007/s10832-021-00263-6.

[84] T. J. Shaffner, "Semiconductor characterization and analytical technology," *Proc. IEEE*, vol. 88, no. 9, pp. 1416–1437, 2000, doi: 10.1109/5.883315.

[85] "Modified Scherrer Equation to Estimate More Accurately Nano-Crystallite Size Using XRD." https://www.scirp.org/journal/paperinformation.aspx?paperid=23195 (accessed May 21, 2023).

[86] M. Tebyetekerwa *et al.*, "Mechanisms and applications of steady-state photoluminescence spectroscopy in two-dimensional transition-metal dichalcogenides," *ACS Nano*, vol. 14, no. 11, pp. 14579–14604, 2020, doi:

10.1021/acsnano.0c08668.

[87] "Transmission electron microscopy (TEM): TEM versus STEM and HAADF - Chemistry LibreTexts." https://chem.libretexts.org/Courses/Franklin_and_Marshall_College/Introduction_to_Materials_Characterization__CHM_412_Collaborative_Text/Electron_and_Probe_Microscopy/Transmission_electron_microscopy_(TEM)%3A_TEM_versus_STEM_and_HAADF (accessed May 21, 2023).

[88] D. B. Williams and C. B. Carter, *Lenses, Apertures, and Resolution*. 1996.

[89] "UV-Vis Spectroscopy: Principle, Strengths and Limitations and Applications | Technology Networks." https://www.technologynetworks.com/analysis/articles/uv-vis-spectroscopy-principle-strengths-and-limitations-and-applications-349865 (accessed May 21, 2023).

[90] G. Benno and J. Kopp, "Optical Properties of Thin Semiconductor Films."

[91] S. Polivtseva *et al.*, "Solution-Mediated Inversion of SnSe to Sb2Se3 Thin-Films," *Nanomaterials*, vol. 12, no. 17, 2022, doi: 10.3390/nano12172898.

[92] S. Polivtseva *et al.*, "A novel thermochemical metal halide treatment for high-performance Sb2Se3 photocathodes," *Nanomaterials*, vol. 11, no. 1, pp. 1–14, 2021, doi: 10.3390/nano11010052.

[93] R. D. Shannon, "Revised Effective Ionic Radii and Systematic Studies of Interatomic Distances in Halides and Chalcogenides," *Acta Cryst.*, vol. A32, pp. 751–767, 1976.

[94] J. Krustok, J. Raudoja, J. H. Schön, M. Yakushev, and H. Collan, "Role of deep donor-deep acceptor complexes in CIS-related compounds," *Thin Solid Films*, vol. 361, pp. 406–410, 2000, doi: 10.1016/S0040-6090(99)00756-7.

[95] J. Krustok, "Photoluminescence from deep acceptor-deep donor complexes in CdTe," *J. Lumin.*, no. 72–74, pp. 103–105, 1997.

[96] M. Grossberg, O. Volobujeva, A. Penežko, R. Kaupmees, T. Raadik, and J. Krustok, "Origin of photoluminescence from antimony selenide," *J. Alloys Compd.*, vol. 817, pp. 1–5, 2020, doi: 10.1016/j.jallcom.2019.152716.